Predicting Regional Pattern of Longitudinal β-Amyloid Accumulation by Baseline PET

Tengfei Guo*[1], Matthias Brendel*[2], Timo Grimmer[3], Axel Rominger*[2], and Igor Yakushev*[1,4]; for the Alzheimer's Disease Neuroimaging Initiative

[1]Department of Nuclear Medicine, Technische Universität München, Munich, Germany; [2]Department of Nuclear Medicine, University of Munich, Munich, Germany; [3]Department of Psychiatry and Psychotherapy, Technische Universität München, Munich, Germany; and [4]Neuroimaging Center at Technische Universität München (TUM-NIC), Munich, Germany

Knowledge about spatial and temporal patterns of β-amyloid (Aβ) accumulation is essential for understanding Alzheimer disease (AD) and for design of antiamyloid drug trials. Here, we tested whether the regional pattern of longitudinal Aβ accumulation can be predicted by baseline amyloid PET. **Methods:** Baseline and 2-y follow-up ^{18}F-florbetapir PET data from 58 patients with incipient and manifest dementia due to AD were analyzed. With the determination of how fast amyloid deposits in a given region relative to the whole-brain gray matter, a pseudotemporal accumulation rate for each region was calculated. The actual accumulation rate of ^{18}F-florbetapir was calculated from follow-up data. **Results:** Pseudotemporal measurements from baseline PET data explained 87% ($P < 0.001$) of the variance in longitudinal accumulation rate across 62 regions. The method accurately predicted the top 10 fast and slow accumulating regions. **Conclusion:** Pseudotemporal analysis of baseline PET images is capable of predicting the regional pattern of longitudinal Aβ accumulation in AD at a group level. This approach may be useful in exploring spatial patterns of Aβ accumulation in other amyloid-associated disorders such as Lewy body disease and atypical forms of AD. In addition, the method allows identification of brain regions with a high accumulation rate of Aβ, which are of particular interest for antiamyloid clinical trials.

Key Words: Alzheimer's disease; amyloid imaging; mild cognitive impairment; dementia; clinical trial

PET with amyloid tracers is an accurate tool for in vivo measurement of neuritic β-amyloid (Aβ) plaques, a pathologic hallmark of Alzheimer disease (AD) (*1*). Beside typical AD, a significant amount of Aβ deposition was found in patients with Lewy body disease (*2*), atypical forms of AD, and mixed dementia (*3*). Importantly, Aβ plaques do not affect the brain uniformly. Rather, they accumulate particularly in the frontal, parietal, and temporal cortices (*4–6*). These are commonly ac-

cepted as AD-typical regions for Aβ accumulation (*7*). Consequently, they are commonly treated as target regions in antiamyloid drug trials (*4,8–10*).

Knowledge about regional pattern of Aβ accumulation is essential for understanding AD and Aβ-associated dementing disorders as well as for the design of antiamyloid drug trials. A repeated amyloid PET scan of the same subject over time is an ideal way to acquire such data. However, large-scale PET studies are expensive and subject to radiation exposure, especially when individuals with mild disease are involved. Realization of such studies is even more problematic in rare as compared with (typical) AD disorders such as in Lewy body disease and atypical forms of AD. In line with this view, no longitudinal PET studies in these Aβ-associated disorders have been published so far.

Here, we tested whether baseline amyloid PET data predict the regional pattern of longitudinal Aβ deposition in AD using a pseudotemporal image analysis. If effective, such an approach could provide preliminary information on spatiotemporal patterns of Aβ deposition in other Aβ-associated disorders.
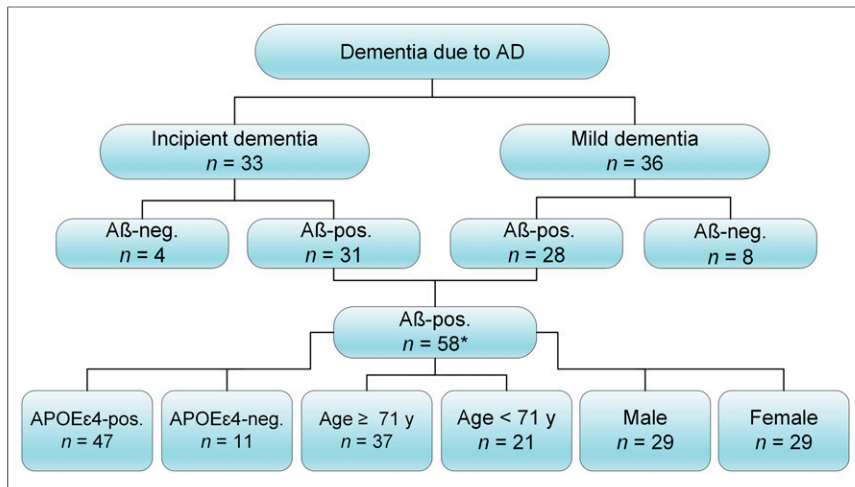
MATERIALS AND METHODS

Participants

The data were obtained from the Alzheimer Disease Neuroimaging Initiative (ADNI) database (ida.loni.usc.edu). The ADNI study was approved by institutional review boards of all participating centers, and written informed consent was obtained from all participants or authorized representatives. Considered were all patients with incipient and mild dementia due to AD, for whom structural MRI, baseline, and 2-y follow-up (FU) ^{18}F-florbetapir PET scans were available. Subjects with incipient AD were those diagnosed with late mild cognitive impairment at the time of baseline florbetapir scanning but who converted to dementia due to AD within 2 y of FU. To ensure the presence of AD pathology, only patients with an amyloid-positive PET scan at baseline were included (*11*). Inclusion of clinically manifest patients with AD resulted in a homogeneous dataset in respect to both clinical phenotype and underlying pathology. Aβ positivity was determined according to the SUV ratio (SUVR) in AD-typical regions with a threshold of greater 1.11 as described elsewhere (*7*) and on the ADNI website (ida.loni.usc.edu). In particular, SUVR in the AD-typical regions was calculated by creating a conventional average across the frontal, anterior/posterior cingulate, lateral parietal, and lateral temporal regions and dividing by the value in the whole cerebellum. Thus, of 69 initially selected patients, 59 were Aβ-positive. After exclusion of 1 significant outlier (Grubbs' test (*12*); Graph-Pad Software), 58 patients remained for further analyses (Fig. 1). The outlier was a
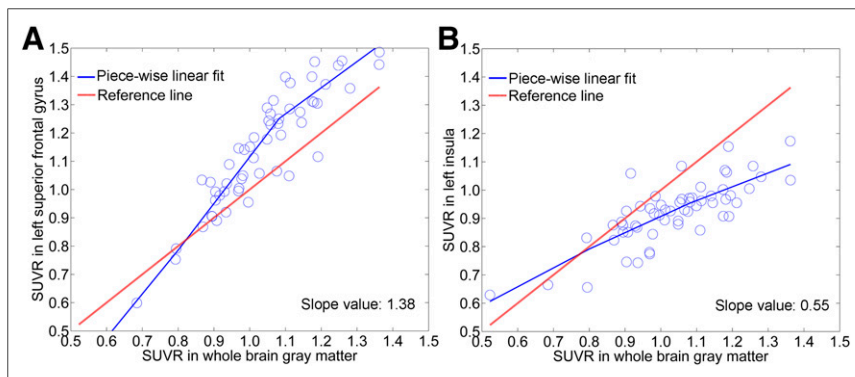
FIGURE 1. Algorithm of data selection. Aβ-pos. and Aβ-neg. denote Aβ-positive and Aβ-negative subjects, respectively. *One subject was excluded as significant outlier.

subject with a 40% reduction in SUVR at FU as compared with baseline PET. To explore potential influence of the apolipoprotein E ε4 (APOE ε4) status, age, and sex on results, subgroup analyses were performed.

Image Data Acquisition and Analysis

Details on image acquisition are given elsewhere (http://adni-info.org). Briefly, PET data were acquired at 50–70 min after injection as 4 × 5 min frames. Images were realigned, averaged, resliced to a common voxel size (1.5 mm³), and smoothed to a common resolution of 8 mm³ in full width at half maximum.

Images were analyzed using the PMOD PNEURO tool (version 3.5; PMOD Technologies). First, PET images were rigidly coregistered to the corresponding MR images. Then, individual MR images were nonlinearly coregistered to the standard MRI template in the Montreal Neurologic Institute (MNI) space. Finally, registration parameters were applied to corresponding PET images. Individual T1-weighted MR images were segmented into gray matter (GM), white matter, and cerebrospinal fluid (*13*) to generate a total of 83 volumes of interest (*14*). Of 83 volumes of interest, 74 were GM regions. Of these, 62 regions with a volume above 1 cm³, that is, 2 × full width at half maximum, were included in the final analyses.

A volume of interest–based correction for partial-volume effects was performed (*15*). Regional SUVR was calculated as ratio of florbetapir uptake in each region to that in white matter (*16,17*). SUVR in whole-brain GM was calculated as a volume-weighted mean value of 62 GM regions, likewise intensity normalized to white matter.

Pseudotemporal Image Analysis

Sixty-two regional SUVR values from the baseline ^{18}F-florbetapir PET were used for the pseudotemporal analysis. Specifically, subjects were ranked according to their SUVR in whole-brain GM (SUVR-GM), resulting in an across-subject waveform for each region (*18*). For a given region r, the SUVRs for n subjects can be expressed as:

$$\text{SUVR}_r(i), i = 1 \ldots n \qquad \text{Eq. 1}$$

where $\text{SUVR}_r(i)$ denotes the SUVR of the ith subject for region r. Then, SUVR_r may be organized by ranking corresponding individual SUVR-GMs from minimal to maximal value, forming a pseudotemporal waveform W_r

$$W_r(j) = \left[\text{SUVR}^{(1)}_{\text{SUVR} - \text{GM(min)}}, \ldots, \text{SUVR}^{(n)}_{\text{SUVR} - \text{GM(max)}} \right], j = 1 \ldots n,$$
$$\text{Eq. 2}$$

where $W_r(j)$ denotes the jth element of W_r.

The assumption behind is that there is a spatial spread of amyloid deposition with disease progression. With the determination of how fast amyloid deposits in a given region relative to whole-brain GM, the pseudotemporal accumulation rate can be extracted. To this end, each region's waveform was fitted using a piecewise linear fit. Each fit was modeled with a restricted linear spline with 4 knots to allow the fitted line varying nonlinearly with total amyloid burden. Examples of piecewise linear fit of a fast-accumulating region (FAR) and a slow-accumulating region (SAR) are given in Figure 2. Subsequently, a derivative function of the fitted line was obtained for each region. Finally, a mean slope value across 58 subjects was calculated for each region according to the derivative function.

FIGURE 2. Piecewise linear fit of pseudotemporal waveforms for FAR (A, left superior frontal gyrus) and SAR (B, left insula). Reference line corresponds to SUVR in whole-brain GM, with a slope value of 1.0.

Regression Analyses

The annual accumulation rate (AAR) of Aβ was calculated as the following:

$$\text{AAR} = \frac{\text{SUVR}_{\text{FU}} - \text{SUVR}_{\text{BL}}}{\text{FU time}}, \qquad \text{Eq. 3}$$

where SUVR_{FU} is the SUVR of the FU PET data, SUVR_{BL} is baseline, and FU time (y) is the time between 2 PET scans. The mean AAR across subjects was calculated for each region.

A linear regression analysis was performed to predict the AAR (as dependent variable) by slope values (as independent variable) across 62 regions. The same analysis was performed in subgroups of subjects stratified according to age, sex, and APOE ε4 status. For the former, the age of 71 y was used as cutoff (*19*).

TABLE 1
Demographic Information for Each Group

Group	n	FU (y)	Age (y)	Sex (F/M)	Education (y)	APOE ε4–positive (%)	Mini-Mental State Examination	Alzheimer's disease assessment scale-cognitive subscale
Incipient dementia	30	1.97 ± 0.12	70.67 ± 7.91	16/14	16.33 ± 2.70	73%	24.87 ± 2.79	19.77 ± 6.80
Mild dementia	28	2.00 ± 0.10	75.25 ± 7.37	13/15	14.96 ± 2.83	89%	21.57 ± 2.17	31.71 ± 10.64
All patients	58	1.99 ± 0.11	72.88 ± 7.93	29/29	15.67 ± 2.82	81%	23.28 ± 3.00	25.53 ± 10.65

For a reference, we in addition performed a linear regression analysis using baseline SUVR and the ratio of baseline SUVR to SUVR-GM as independent variables.

FARs and SARs

To explore the utility of these analyses in the context of clinical trials, we determined FARs and SARs according to ranks of both longitudinal (AARs) and baseline (slope values) measurements. The top 10 FARs were combined into a single composited FAR according to Equation 4 and were treated as a putative target in clinical trials, followed by a comparison with the commonly used set of AD-typical regions. This set consisted of 18 regions, covering the frontal (8 regions), parietal (3 regions including precuneal/posterior cingulate), and temporal (6 regions) lobes (16) plus the anterior cingulate region.

When separated into subgroups with incipient ($n = 30$) and mild ($n = 28$) dementia due to AD, the prediction was still strong, with an R^2 of 0.77 and 0.58 ($P < 0.001$ for both), respectively. The regression remained highly significant after stratification according to age, sex, and the APOE ε4 status ($P < 0.001$ for all, Table 2).

In the whole cohort, baseline SUVR and the ratio baseline SUVR/SUVR-GM predicted AARs with a similar accuracy ($R^2 = 0.53$ and 0.49, respectively, $P < 0.001$ for both). When slope values and baseline SUVR were introduced into a forced (baseline SUVR first) stepwise linear regression analysis, slope values explained an additional, significant amount of variance (R^2 change $= 0.35$, $P < 0.001$).

$$\text{SUVR-composited} = \frac{\left(\text{SUVR}_{region(1)} \times \text{Volume}_{region(1)} + \cdots + \text{SUVR}_{region(K)} \times \text{Volume}_{region(K)} \ldots + \text{SUVR}_{region(N)} \times \text{Volume}_{region(N)}\right)}{\left(\text{Volume}_{region(1)} + \cdots + \text{Volume}_{region(K)} \cdots + \text{Volume}_{region(N)}\right)}, \quad \text{Eq. 4}$$

where $\text{SUVR}_{region(K)}$ is the SUVR of Kth region, $\text{Volume}_{region(K)}$ is the volume of Kth region, and SUVR-composited is the SUVR of composited FAR, AD-typical regions, or whole-brain GM.

Statistical Analysis

The normality of distribution was tested using the D'Agostino–Pearson test (Graph-Pad Software) and visual inspection of variable histograms. Data are presented as mean ± SD. The mean AAR of the composited FAR across 58 subjects was compared with those of whole-brain GM and AD-typical regions using a 2-tailed paired-sample t test. Statistical significance was defined as a P value of less than 0.05. Regression and statistical analyses were performed using SPSS for Windows (version 22.0).

RESULTS

Demographic data of patients at baseline are summarized in Table 1.
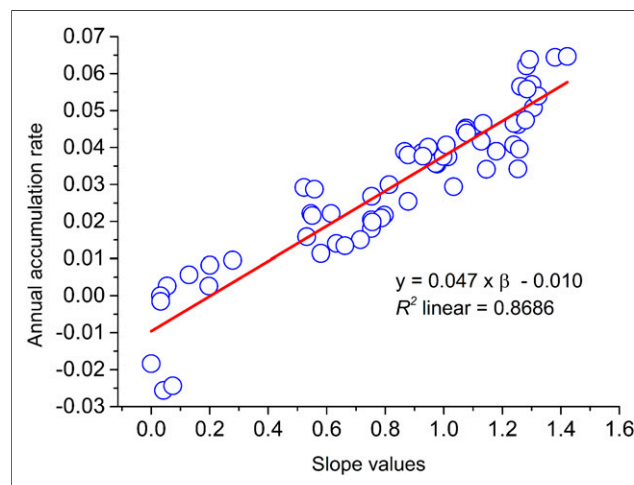
Regression Analysis

As illustrated in Figure 3, slope values accurately predicted AARs across 62 regions ($R^2 = 0.87$, $P < 0.001$) following the function:

$$y = 0.047 \times \beta - 0.010, \quad \text{Eq. 5}$$

where y indicates AAR, and β means the slope value of each region.

FARs and SARs

Bilateral anterior cingulate, superior, and middle frontal gyri, left superior parietal, anterior orbital, and posterior cingulate regions, and inferiolateral remainder of the parietal lobe were found to be top 10 FARs (Table 3). These 10 regions were combined into the composited FAR according to the Equation 4 (Fig. 4).

FIGURE 3. Linear regression across 62 regions.

TABLE 2
Linear Regression Coefficient (Pearson) Between Pseudotemporal and Longitudinal Measurements in Subgroups of Patients

Subgroup	APOE ε4– positive	APOE ε4– negative	Age ≥ 71 y	Age < 71 y	Male	Female
n	47	11	37	21	29	29
R^2	0.82	0.32	0.72	0.58	0.79	0.70

Bilateral hippocampus, caudate nucleus, thalamus, amygdala, and parahippocampal gyrus appeared to be the top 10 SARs (Supplemental Table 1). Notably, 10 regions with the highest AAR were the same 10 regions with the largest fitted line slope. The same was true for the 10 regions with the lowest AAR.

The mean slope of the composited FAR was 1.31 ± 0.15—that is, higher than those of the composited AD-typical regions (slope = 1.15 ± 0.12) and whole-brain GM (slope = 1.0) (Fig. 5A). The mean AAR of the composited FAR was 0.057 ± 0.045. The mean AARs of whole-brain GM and AD-typical regions were significantly lower, that is, 0.039 ± 0.032 ($P < 0.001$) and 0.046 ± 0.038 ($P < 0.001$), respectively (Fig. 5B). Assuming a roughly linear relationship between Aβ and time in amyloid-positive subjects (20,21), SUVR of the composited FAR increased 1.48 and 1.24 times faster than that of the whole-brain GM and AD-typical regions, respectively (Fig. 5C). Thus, the composited FAR can reduce duration of a 2-y drug trial by approximately 32% and 19%, respectively.
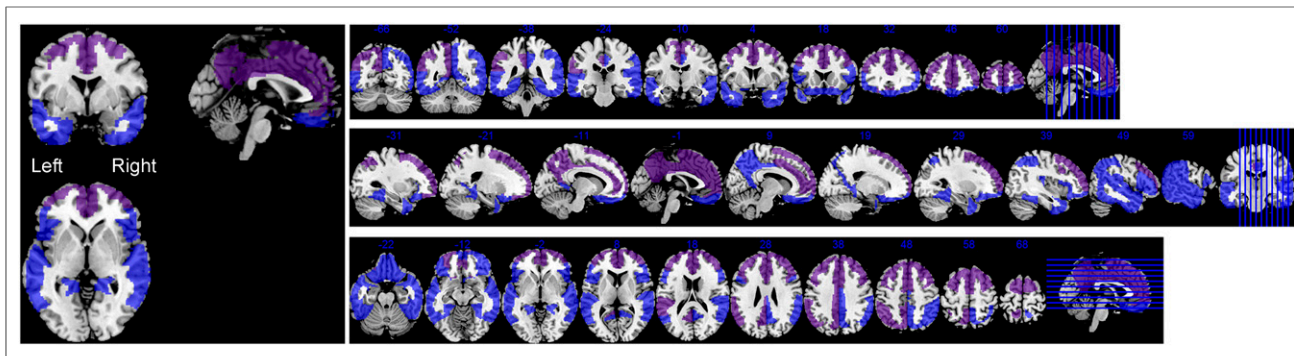
DISCUSSION

In this study, we tested whether baseline PET data can predict the regional pattern of Aβ accumulation over 2 y. In a group of patients with incipient and mild Alzheimer dementia, baseline ^{18}F-florbetapir measurements from a pseudotemporal image analysis explained 87% of the variance in AARs across 62 regions. The results were consistent throughout the disease severity (incipient or manifest dementia), age intervals, genders, and the APOE genotypes.

TABLE 3
Fast-Accumulating Regions (FARs)

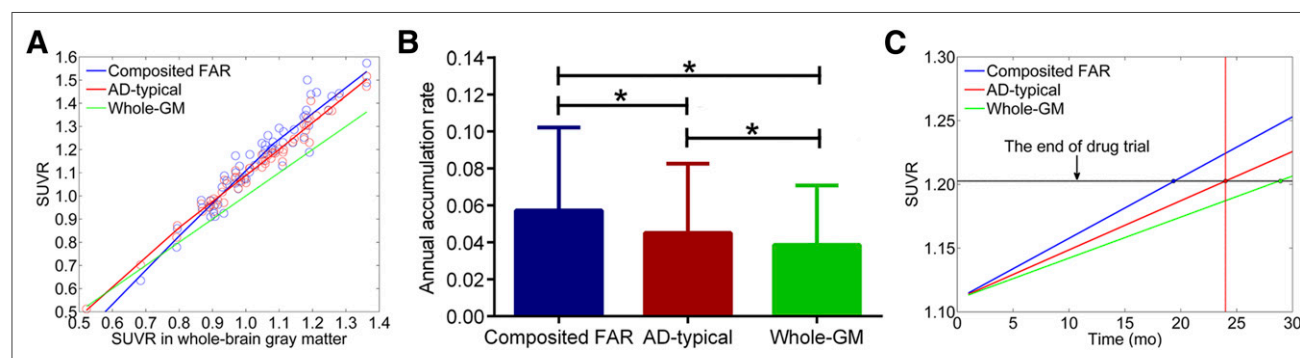| Region	Rank of slope	Slope	Rank of AAR	AAR (mean ± SD)	Volume (mm³)
Anterior cingulate gyrus_L	1	1.42	1	0.0646 ± 0.0621	7,747
Superior frontal gyrus_L	2	1.38	2	0.0644 ± 0.0565	46,866
Superior parietal gyrus_L	3	1.32	8	0.0540 ± 0.0505	38,141
Anterior orbital gyrus_L	4	1.31	9	0.0508 ± 0.0636	5,164
Superior frontal gyrus_R	5	1.30	5	0.0571 ± 0.0614	46,158
Anterior cingulate gyrus_R	6	1.29	3	0.0638 ± 0.0515	7,441
Posterior cingulate gyrus _L	7	1.28	7	0.0558 ± 0.0598	7,159
Middle frontal gyrus_R	8	1.28	4	0.0621 ± 0.0534	42,929
Inferiolateral remainder of parietal lobe_L	9	1.28	10	0.0474 ± 0.0479	37,662
Middle frontal gyrus_L	10	1.26	6	0.0566 ± 0.0500	44,690
Posterior superior temporal gyrus_L	11	1.26	22	0.0396 ± 0.0633	12,220
Lateral remainder of occipital lobe_L	12	1.25	13	0.0462 ± 0.0547	38,030
Cuneus_L	13	1.25	33	0.0342 ± 0.0560	9,438
Superior parietal gyrus_R	14	1.24	11	0.0465 ± 0.0492	37,509
Anterior orbital gyrus_R	15	1.24	19	0.0407 ± 0.0686	4,807
Lateral remainder of occipital lobe_R	16	1.18	23	0.0390 ± 0.0424	38,789
Lingual gyrus_L	17	1.15	34	0.0341 ± 0.0529	12,333
Postcentral gyrus_L	18	1.13	12	0.0465 ± 0.0550	23,201
Inferiolateral remainder of parietal lobe_R	19	1.13	18	0.0417 ± 0.0450	38,214
Inferior frontal gyrus_R	20	1.12	17	0.0439 ± 0.0526	15,294
Posterior superior temporal gyrus_R	21	1.08	16	0.0440 ± 0.0665	12,468
Inferior frontal gyrus_L	22	1.08	14	0.0453 ± 0.0597	14,448
Postcentral gyrus_R	23	1.07	15	0.0448 ± 0.0550	25,731
Cuneus_R	24	1.03	36	0.0294 ± 0.0548	9,224
Posterior cingulate gyrus_R	25	1.01	30	0.0375 ± 0.0487	7,557
Posterior temporal lobe_L	26	1.01	20	0.0407 ± 0.0393	44,469
Whole-brain GM	27	1	26	0.0386 ± 0.0321	851,002

_L = left; _R = right.

FIGURE 4. Composited FAR (purple) and AD-typical regions (blue) as overlaid onto standard T1 MRI template in MNI space. Composited FAR region fully overlaps with AD-typical regions.

A pseudotemporal analysis was initially reported by Braak and Braak, who studied progression of Aβ deposition in cross-sectional data from postmortem brain tissue (22). Recently, a pseudotemporal analysis of PET images has been applied at the voxel level (18). Assuming that total amyloid burden would be a reasonable approximation of the disease severity, Yotter et al. (18) estimated spatial patterns of the longitudinal Aβ accumulation from cross-sectional image data. The authors found that the pseudotemporal pattern of regional Aβ deposition was stronger related to cognitive function of healthy elderly individuals than total amyloid burden (18). Although their results were plausible, they were not validated against real longitudinal data. In the present study, we adopted the method of Yotter et al. for region-based analyses and verified its efficacy using longitudinal data in clinically manifest AD.

The core of our finding is a positive, linear relationship between baseline measurements of Aβ and their longitudinal changes across regions. Thus, 55% of the variance in AARs could be explained by baseline tracer uptake. In other words, regions with a high/low baseline Aβ load are also those with a high/low AAR at the stage of clinically manifest AD. It is important to distinguish this approach from an across-subject paradigm, in which baseline measurements of whole-brain uptake are correlated with longitudinal measurements of whole-brain tracer uptake across subjects, for example (21). Such studies found a slowing of Aβ accumulation rate at the advanced stage of AD (21). Our results do not contradict these findings. Whereas the Aβ accumulation rate in the whole brain might be slowing in advanced AD, some brain regions can still continue to accumulate Aβ. Further, no patients with advanced/severe or even moderate Alzheimer dementia were included in the present study.

As shown by a stepwise linear regression analysis, slope values explained significantly more variance (+35%) in AAR than baseline SUVR alone, demonstrating the power of the proposed approach. This is plausible, because slope values contain pseudotemporal information about the dynamics of Aβ deposition in a given region. Remarkably, the pseudotemporal image analysis revealed the same FARs and SARs as the longitudinal analysis. Namely, the bilateral anterior cingulate, superior, and middle frontal gyri; left superior parietal, anterior orbital, and posterior cingulate; and inferiolateral remainder of the parietal lobe were found to have the largest slope and the highest AAR. By contrast, the bilateral hippocampus, caudate nucleus, thalamus, amygdala, and parahippocampal gyri had the smallest slope and the lowest AAR. Our findings are well in line with those of Grimmer et al. (23), who examined regional progression of Aβ in Alzheimer dementia using PET with Pittsburgh compound B (23). As in our study, they found that regions of the frontal lobe followed by those of the parietal lobe showed the highest accumulation rate, whereas the temporal lobe appeared to have the lowest rate across the neocortex. Further, most of the FARs accumulated Aβ faster in the left hemisphere (23). The same order of accumulation rate (frontal > parietal > occipital > temporal) was found by Rinne et al. (4). However, other groups found the lateral temporal cortex to be a

FIGURE 5. (A) Pseudotemporal analysis of 3 sets of regions. Green line is reference fit, with slope value of 1.0. (B) Annual accumulation rates (mean ± SD) for composited FAR, AD-typical regions, and whole-brain GM. *$P < 0.001$ in a 2 tailed paired t test. (C) Three sets of regions as putative targets in hypothetical drug trial of 24 mo.

FAR (5,6). Somewhat unexpectedly, we observed the posterior cingulate region to accumulate Aβ slower than the anterior cingulate region. Although this is still consistent with some reports (23), a few studies reported the posterior cingulate cortex to be one of the most active Aβ-accumulating regions (4,24). The discrepancy may well be related to methodologic factors such as lack of partial-volume correction (4,24) and different reference regions (4,5,24). Most longitudinal studies with amyloid PET measured SUVR either in the whole brain or in the AD-typical regions, without a detailed regional analysis. As for the SARs, only Grimmer et al. (23) conducted a similarly detailed analysis including 90 volumes of interest. In line with our findings, they reported low or no increases in Aβ accumulation in the archipallium, thalamus, and caudate nucleus (23).

Aβ deposition is a slow process, likely extending for more than 2 decades (20,21). This around 20-y interval provides a large therapeutic window. So far, no longitudinal amyloid PET study in atypical AD, Lewy body disease, or mixed (AD and vascular) diseases has been reported. Thus, our approach can be used to predict regional patterns of Aβ accumulation in these clinical entities. In particular, the proposed method can predict regions with the highest Aβ accumulations rate, which are of interest for antiamyloid clinical trials. In the present study, the set of AD-typical regions was found to have a higher Aβ AAR than the whole-brain GM, confirming the relevance of these regions in AD. However, the pseudotemporal analysis revealed a set of regions with a significantly higher accumulation rate of Aβ than AD-typical regions. Consequently, when used as a target region, the duration of a drug trial can be reduced by approximately 19% as compared with AD-typical regions.

There is an increasing number of longitudinal studies in asymptomatic subjects with or at risk for AD by virtue of a mutation (25,26), gene status (27,28), or significant amyloid burden as measured by PET (29,30) or cerebrospinal fluid analyses (31). Although highly interesting from the perspective of clinical trials, we did not include asymptomatic individuals in the present study, because their clinical fate is unclear. Indeed, the presence of a significant Aβ load does not mean a future development of (typical) clinical AD. Instead, the subject may have a mixed dementing disorder, Lewy body disease, or an atypical AD. Thus, if such subjects were included in the present study, we might have a heterogeneous sample of patients with unclear clinical phenotype, as well as with distinct spatial patterns of Aβ accumulation. In a similar vein, to ensure the presence of the AD pathology as origin of the clinical phenotype, this study included only patients with an amyloid-positive baseline PET scan. Yet, the proposed method can be effective in amyloid-negative subjects, too. Such an approach would allow capturing the whole trajectory of Aβ accumulation, including a long preclinical phase. Given uncertainty about both pathologic and clinical pathways, however, interpretation of results would be problematic.

A limitation of the present study is that only 2-y FU data were available. Although the relationship between baseline and longitudinal measurements of Aβ deposition was strong, the correspondence at the level of individual regions was far from perfect, especially beyond the top 10 FARs and SARs. This may well be explained by the short FU period, which is incomparable with the disease duration as captured by the pseudotemporal image analysis. Thus, one would expect a larger correspondence between the measurements when a longer FU is available. Further, our results with respect to FARs are limited to amyloid-positive patients with clinically manifest AD. Thus, FARs may in part differ in amyloid-negative and asymptomatic subjects. Finally, the present results should be replicated in an independent sample of patients.

CONCLUSION

The pseudotemporal analysis of baseline PET images is capable of predicting a regional pattern of longitudinal Aβ accumulation in clinically manifest AD at a group level. This approach may be useful in exploring spatial patterns of Aβ accumulation in other amyloid-associated disorders such as Lewy body disease and atypical forms of AD. In addition, the method allows identification of brain regions with a high accumulation rate of Aβ, which are of particular interest for antiamyloid drug trials.

DISCLOSURE

ACKNOWLEDGMENTS

REFERENCES

1. Clark CM, Pontecorvo MJ, Beach TG, et al. Cerebral PET with florbetapir compared with neuropathology at autopsy for detection of neuritic amyloid-β plaques: a prospective cohort study. *Lancet Neurol.* 2012;11:669–678.

2. Gomperts SN, Locascio JJ, Marquie M, et al. Brain amyloid and cognition in Lewy body diseases. *Mov Disord.* 2012;27:965–973.

3. Lee JH, Kim SH, Kim GH, et al. Identification of pure subcortical vascular dementia using ^{11}C-Pittsburgh compound B. *Neurology.* 2011;77:18–25.

4. Rinne JO, Brooks DJ, Rossor MN, et al. 11 C-PiB PET assessment of change in fibrillar amyloid-β load in patients with Alzheimer's disease treated with bapineuzumab: a phase 2, double-blind, placebo-controlled, ascending-dose study. *Lancet Neurol.* 2010;9:363–372.

5. Villemagne VL, Pike KE, Chetelat G, et al. Longitudinal assessment of Abeta and cognition in aging and Alzheimer disease. *Ann Neurol.* 2011;69: 181–192.

6. Villain N, Chetelat G, Grassiot B, et al. Regional dynamics of amyloid-beta deposition in healthy elderly, mild cognitive impairment and Alzheimer's disease: a voxelwise PiB-PET longitudinal study. *Brain.* 2012;135:2126–2139.

7. Landau SM, Mintun MA, Joshi AD, et al. Amyloid deposition, hypometabolism, and longitudinal cognitive decline. *Ann Neurol.* 2012;72:578–586.

8. Salloway S, Sperling R, Fox NC, et al. Two phase 3 trials of bapineuzumab in mild-to-moderate Alzheimer's disease. *N Engl J Med.* 2014;370:322–333.

9. Siemers ER, Sundell KL, Carlson C, et al. Phase 3 solanezumab trials: secondary outcomes in mild Alzheimer's disease patients. *Alzheimers Dement.* 2016;12: 110–120.

10. Liu E, Schmidt ME, Margolin R, et al. Amyloid-β ^{11}C-PiB-PET imaging results from 2 randomized bapineuzumab phase 3 AD trials. *Neurology.* 2015;85:692–700.

11. McKhann GM, Knopman DS, Chertkow H, et al. The diagnosis of dementia due to Alzheimer's disease: recommendations from the National Institute on Aging-Alzheimer's Association workgroups on diagnostic guidelines for Alzheimer's disease. *Alzheimers Dement.* 2011;7:263–269.

12. Grubbs FE. Procedures for detecting outlying observations in samples. *Technometrics.* 1969;11:1–21.

13. Ashburner J, Friston KJ. Unified segmentation. *Neuroimage.* 2005;26:839–851.

14. Hammers A, Allom R, Koepp MJ, et al. Three-dimensional maximum probability atlas of the human brain, with particular reference to the temporal lobe. *Hum Brain Mapp.* 2003;19:224–247.

15. Rousset OG, Collins DL, Rahmim A, Wong DF. Design and implementation of an automated partial volume correction in PET: application to dopamine receptor quantification in the normal human striatum. *J Nucl Med.* 2008;49:1097–1106.

16. Brendel M, Hogenauer M, Delker A, et al. Improved longitudinal [^{18}F]-AV45 amyloid PET by white matter reference and VOI-based partial volume effect correction. *Neuroimage.* 2015;108:450–459.

17. Chen K, Roontiva A, Thiyyagura P, et al. Improved power for characterizing longitudinal amyloid-β PET changes and evaluating amyloid-modifying treatments with a cerebral white matter reference region. *J Nucl Med.* 2015;56:560–566.

18. Yotter RA, Doshi J, Clark V, et al. Memory decline shows stronger associations with estimated spatial patterns of amyloid deposition progression than total amyloid burden. *Neurobiol Aging.* 2013;34:2835–2842.

19. Fleisher AS, Chen K, Liu X, et al. Apolipoprotein E epsilon4 and age effects on florbetapir positron emission tomography in healthy aging and Alzheimer disease. *Neurobiol Aging.* 2013;34:1–12.

20. Jack CR, Wiste HJ, Lesnick TG, et al. Brain β-amyloid load approaches a plateau. *Neurology.* 2013;80:890–896.

21. Villemagne VL, Burnham S, Bourgeat P, et al. Amyloid β deposition, neurodegeneration, and cognitive decline in sporadic Alzheimer's disease: a prospective cohort study. *Lancet Neurol.* 2013;12:357–367.

22. Braak H, Braak E. Staging of Alzheimer-related cortical destruction. *Int Psychogeriatr.* 1997;9:257–261.

23. Grimmer T, Tholen S, Yousefi BH, et al. Progression of cerebral amyloid load is associated with the apolipoprotein E epsilon4 genotype in Alzheimer's disease. *Biol Psychiatry.* 2010;68:879–884.

24. Engler H, Forsberg A, Almkvist O, et al. Two-year follow-up of amyloid deposition in patients with Alzheimer's disease. *Brain.* 2006;129:2856–2866.

25. Yau W-YW, Tudorascu DL, McDade EM, et al. Longitudinal assessment of neuroimaging and clinical markers in autosomal dominant Alzheimer's disease: a prospective cohort study. *Lancet Neurol.* 2015;14:804–813.

26. Fagan AM, Xiong C, Jasielec MS, et al. Longitudinal change in CSF biomarkers in autosomal-dominant Alzheimer's disease. *Sci Transl Med.* 2014;6:226ra30.

27. Mielke MM, Machulda MM, Hagen CE, et al. Influence of amyloid and APOE on cognitive performance in a late middle-aged cohort. *Alzheimers Dement.* 2016;12:281–291.

28. Bilgel M, An Y, Zhou Y, et al. Individual estimates of age at detectable amyloid onset for risk factor assessment. *Alzheimers Dement.* 2016;12:373–379.

29. Sojkova J, Zhou Y, An Y, et al. Longitudinal patterns of β-amyloid deposition in nondemented older adults. *Arch Neurol.* 2011;68:644–649.

30. Vlassenko AG, Mintun MA, Xiong C, et al. Amyloid-beta plaque growth in cognitively normal adults: longitudinal [^{11}C] Pittsburgh compound B data. *Ann Neurol.* 2011;70:857–861.

31. Vos SJB, Xiong C, Visser PJ, et al. Preclinical Alzheimer's disease and its outcome: a longitudinal cohort study. *Lancet Neurol.* 2013;12:957–965.